Interactions between Josephson vortices and breathers

E. Trías,[1] J. J. Mazo,[2,3] and T. P. Orlando[1]
[1]*Department of Electrical Engineering and Computer Science, Massachusetts Institute of Technology, Cambridge, Massachusetts 02139*
[2]*Departamento de Física de la Materia Condensada, Universidad de Zaragoza, E-50009, Zaragoza, Spain*
[3]*Departamento de Teoría y Simulación de Sistemas Complejos, Instituto de Ciencia de Materiales de Aragón, CSIC-Universidad de Zaragoza, E-50009, Zaragoza, Spain*
(Received 9 June 2001; published 15 January 2002)

We study vortex-breather collisions in a Josephson-junction ladder array. We have computed parameters values of the system for which both types of structures coexist in the ladder. In order of increasing bias current, we have found different possible scenarios for vortex-breather collisions. (i) At low bias current, the breather acts as a pinning center for a single vortex. (ii) Increasing the current, the vortex excites multisite breathers in its wake and is finally pinned by the breather. (iii) At still higher current, a whirling mode front is excited by the vortex. However, the breather still acts as a pinning center, but now for the front. (iv) At higher values of the bias, the front is able to destroy the breather. For scenario (i), we have also studied thermal activation properties associated with the presence of the vortex-breather pair in the array.

DOI: 10.1103/PhysRevB.65.054517 PACS number(s): 74.50.+r, 05.45.−a, 63.20.Pw, 85.25.Cp

I. INTRODUCTION

The nonlinear dynamical concept of *coherent structures* or *coherent excitations* has important consequences when applied to condensed matter systems.[1] Spatially or temporally coherent structures appear in many nonlinear extended systems. Such structures usually can be characterized by marked particlelike properties. In the past few years, these notions have become fundamental for understanding many problems and their implications extend over different fields of the physics of continuous and discrete systems.

In one dimension, the concept of a soliton is applied to intrinsically localized structures with a topological charge. Examples of a soliton are kinks in discrete systems, discommensurations in commensurate-incommensurate transition theory, or fluxons or vortices in Josephson arrays. Recently intrinsic localized modes without topological charge, known also as *discrete breathers* (DB's), have been studied.[2–4] A DB corresponds to a dynamical solution of a discrete nonlinear system for which energy remains spatially localized in the lattice. In a single-site DB the order parameter describes large amplitude oscillations or rotations on one of the sites of the lattice while small amplitude oscillations occur on the other sites. This localization is intrinsic and generic in homogeneous nonlinear discrete systems and does not carry any associated topological charge.

Linking the subjects of coherent structures and the physics of condensed matter systems and devices, Josephson-junction- (JJ-) based arrays provide an almost ideal experimental system to test many of these nonlinear concepts. This is because JJ's are solid-state realizations of nonlinear oscillators which can be easily coupled using standard lithographic techniques. Indeed, many experimental studies in the field have been devoted to investigate the static and propagation properties of vortices in long and small JJ arrays in their classical[5–8] or quantum regimes.[9]

Recently, small JJ arrays have been successfully designed for the experimental study of a large family of DB solutions named rotating localized modes or rotobreathers. These rotobreathers have been detected in arrays with a ladder geometry driven by dc external currents[10–13] and are robust against thermal and other fluctuations. Interestingly, as predicted[14] families of solutions with different voltage symmetries were found.

In this paper we will numerically study the simplest interaction that occurs when a moving vortex collides with a stationary rotobreather. We first will briefly review the description of the system and the simulated equations for the dynamics of the ladder. Then we present four different scenarios of collisions of a vortex with a rotobreather. In one of the cases the result of such a collision is a vortex-breather pair. We will then show that a discrete breather acts as a pinning center to vortex motion, study the equilibrium properties of such a pair in the presence of temperature, and calculate an energy barrier associated with the pair. Finally, we dedicate two appendixes to review some of the properties of a single vortex and a DB in a JJ ladder array, because it is necessary to know the parameter values where both a breather and a moving vortex can coexist in a ladder.

II. JOSEPHSON LADDER

Figure 1 shows the circuit diagram for a Josephson ladder array where junctions are marked by an "×." This configuration differs from the parallel array in the presence of hori-

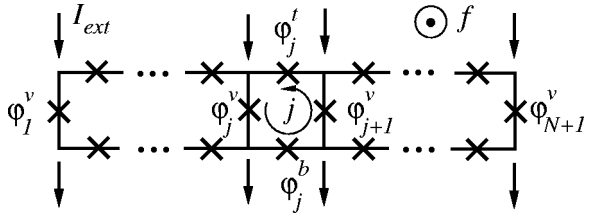

FIG. 1. The anisotropic ladder array with uniform current injection. Vertical junctions (with superscript v) have critical current I_{cv} and horizontal junctions (with superscript t and b) have a critical current I_{ch}.

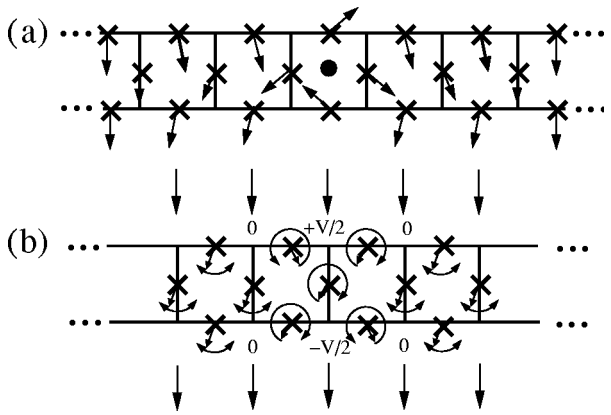

FIG. 2. (a) Sketch of a single-vortex configuration in the ladder at $f=0$ and $I_{\rm ext}=0$. In the absence of an external field this configuration is stable only at small values of λ. (b) Sketch of the single-site DB studied in the paper. The ladder is biased by a dc external current and one vertical and four horizontal junctions rotate while the others librate.

zontal junctions and can be considered the simplest square two-dimensional (2D) array. The JJ parallel array is usually described in terms of the discrete sine-Gordon or Frenkel-Kontorova model,[8] a model which has been paradigmatic for studying kinks and commensurate-incommensurate transitions.[15]

The static properties of a vortex in the ladder are similar to those of a kink in the Frenkel-Kontorova or discrete sine-Gordon system.[16–18] There are, however, some differences, the most important of which is the existence of a critical magnetic field f_c for which, if $f<f_c$, a single vortex is not stable in the ladder.[19] Below this critical field the vortex is expelled from the ladder through the horizontal junctions. Thus vortices are stable static solutions of the array at adequate parameter values and, in the absence of external currents, a static vortex in the ladder corresponds to a solution for which the phase of the vertical junctions φ_j^v go from 0 to 2π [see Fig. 2(a)].

Another important difference between the ladder and parallel array is that when biased by dc external currents a ladder sustains discrete breather solutions. A DB in the ladder corresponds to a dynamical state where one of the vertical junctions is in a resistive rotating state while the others librate around some equilibrium position. Figure 2(b) shows a sketch of such a solution where, in order to satisfy Kirchhoff's voltage law, the four horizontal junctions next to the rotating vertical one also rotate. This configuration is the simplest DB solution within the diversity of states that have been numerically and experimentally found.[10–14] In this paper we will refer to this type of single-site symmetric discrete breather solution where one vertical and four horizontal junctions rotate. Although there are other types of discrete breather solutions, we will set our parameter values to the region of predominance of these symmetric solutions.

The object of this paper is a numerical study of vortex-breather interactions in a JJ ladder array. To carry out our numerical study we need to derive a model for the array. The junctions will be modeled by the parallel combination of an ideal Josephson junction with a critical current of I_c^j, a capacitor C_j, and a resistance R_j. The ideal Josephson junction has a constitutive relation of $I_j=I_c^j\sin\varphi_j$, where φ_j is the gauge-invariant phase difference of the junction. When there is a voltage across the junction, v_j, then $v_j=(\Phi_0/2\pi)d\varphi_j/dt$.

We will also use the standard Langevin approach to include thermal effects. We replace the resistor by a noiseless resistor in parallel with a Johnson current noise source. The Josephson junctions are then modeled by

$$C_j\dot{v}_j+\frac{v_j}{R_j}+I_c^j\sin\varphi_j+I_j^N=I_{\rm ext}, \tag{1}$$

where $\langle I_j^N(t)I_k^N(t')\rangle=(2kT/R_j)\delta(t-t')\delta_{jk}$. This results in the usual current noise spectrum density $S_j=2kT/R_j$.

Anisotropic ladders can be fabricated by varying the area of the horizontal and vertical junctions. The normal-state resistance is inversely proportional to the junction area because of the constant I_cR_n product. We will use I_{ch} for the horizontal junction critical current and I_{cv} for the vertical junction critical current. The anisotropy parameter h can then be defined as $h=I_{ch}/I_{cv}=C_h/C_v=R_v/R_h$.

The open boundaries imply that the current on the top horizontal junctions must be equal but opposite to the current in the bottom horizontal junctions, and this bottom one is equal to the mesh current i_j^m. The junctions in the array are coupled by means of current conservation and fluxoid quantization. After normalizing the currents by I_{cv} we get the following governing-equations in the self-inductance limit:

$$\mathcal{N}(\varphi_j^t)=\frac{\lambda}{h}\{\varphi_j^v-\varphi_{j+1}^v-\varphi_j^t+\varphi_j^b+2\pi f\},$$

$$\mathcal{N}(\varphi_j^v)=\lambda\{\varphi_{j+1}^v-2\varphi_j^v+\varphi_{j-1}^v+\varphi_j^t-\varphi_{j-1}^t-\varphi_j^b+\varphi_{j-1}^b\}+i_{\rm ext},$$

$$\mathcal{N}(\varphi_j^b)=-\frac{\lambda}{h}\{\varphi_j^v-\varphi_{j+1}^v-\varphi_j^t+\varphi_j^b+2\pi f\}. \tag{2}$$

We let the functional $\mathcal{N}(\varphi)=\ddot{\varphi}+\Gamma\dot{\varphi}+\sin\varphi+i_j^n$ represent the current through a junction. The noise spectrum of i_j^n is $S_j=2kTh_j\Gamma/E_J$, where the Josephson energy $E_J=(\Phi_0/2\pi)I_{cv}$ and $h_j=I_c^j/I_{cv}$. The dimensionless temperature is then $\tilde{T}=kT/E_J$. The external current is normalized as $i_{\rm ext}=I_{\rm ext}/I_{cv}$ and f measures, in units of the flux quantum Φ_0, the magnetic field flux through each individual cell. The damping is $\Gamma=\sqrt{\Phi_0/2\pi I_{cv}R_v^2C_v}$. We note that because the anisotropy in our arrays is caused by varying the junction area, Γ is the same for every junction in the array. λ is the ratio between the Josephson inductance and the mesh self-inductance, $\lambda=\Phi_0/(2\pi I_cL)$.

In Eq. (2), $j=1$ to N and, at the open boundaries, $\varphi_0^t=\varphi_N^t=0$, $\varphi_0^b=\varphi_N^b=0$, $\varphi_{N+1}^v=\varphi_N^v+2\pi f$, and $\varphi_0^v=\varphi_1^v-2\pi f$, where the phases at $j=0$ and $j=N+1$ are for mathematical convenience and do not represent real junctions.

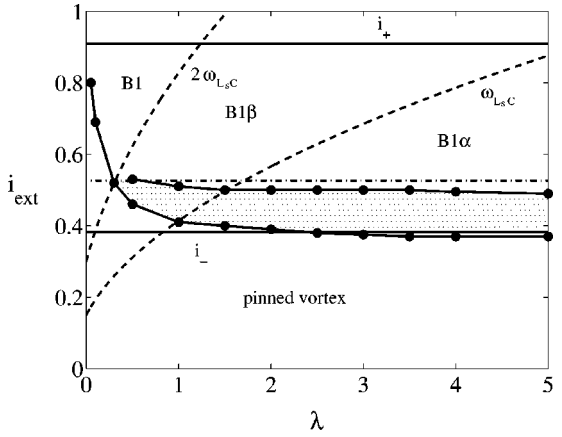

FIG. 3. Existence region of our type of breathers and a single vortex. The hatched region represents the space where a ladder supports a single traveling vortex for $h=0.5$ and $f=0.3$. The dashed lines are ω_{L_sC} and $2\omega_{L_sC}$.

The vorticity n_j is defined through the expression $n_j=(1/2\pi)\{[\varphi_j^v]-[\varphi_{j+1}^v]-[\varphi_j^t]+[\varphi_j^b]\}+f+f_j^{\rm ind}$, where $[\varphi]$ represents the phases modulus 2π and $f_j^{\rm ind}=i_j^m/2\pi\lambda$.

This system of equations has two linearized modes represented by ω_{L_sC} and ω_{L_JC} as explained in Appendix A. In the rest of the article, we will refer to these linear modes as the L_sC and L_JC resonances.

In order to study vortex-breather interactions in the ladder, first we need to study the parameter values (h, Γ, λ, f, and $i_{\rm ext}$) for which DB's and vortices coexist. We present the details of this study in two appendixes. The main conclusion is that there exists a wide region in the parameter space for the coexistence of vortices and DB's in the array.

Figure 3 shows the existence region of a breather and a vortex in ladder. The hatched region shows the parameter space where a single moving vortex can exist in the array. The vortex depins at $i_{\rm dep}$ and as the current increases it destabilizes at $i_{\rm ext}\simeq 0.5$ when the moving vortex resonates with the L_JC resonance (dot-dashed line). The moving vortex can then excite junctions in its wake to rotate. Above this maximum current, the array does not support a single moving vortex and instead the trailing edge of the vortex excites every vertical junction in its wake. This state can be interpreted as an advancing front of a whirling mode.

Figure 3 also shows the existence region for the symmetric discrete breathers studied here. The bottom solid line at $i_{\rm ext}=0.38$ is a rough estimation of the minimum current [as expected from the retrapping mechanism, Eq. (B2)].[20] The top solid line at $i_{\rm ext}=0.91$ is the maximum current of the breather, Eq. (B1). The two curving dashed lines are the L_sC resonances. There are two branches because the horizontal junction rotates at half the voltage of the vertical junction. $B1$, $B1\alpha$, and $B1\beta$ represent different single-site DB solutions.[21] There is also a region in Fig. 3 that allows for aperiodic solutions, but in order to simplify the graph, it is not shown.

As shown in Fig. 3, there is a region in the parameter plane where a DB can coexist with a single vortex in a ladder. It is this overlap that allows us to study interactions between breathers and vortices. This overlap will change with the parameters. For instance, if we increase h, then the depinning current would decrease, but the retrapping current of the breather would increase, so the overlap existence region would be smaller. In the next section we present some results of interaction between breathers and vortices and to avoid any effects of the resonances we let $\lambda=5$ and we will start with $i_{\rm ext}=0.45$. Also, we will set in our simulations $\Gamma=0.1$, $f=0.3$, and $h=0.5$ as explained in Appendix B.

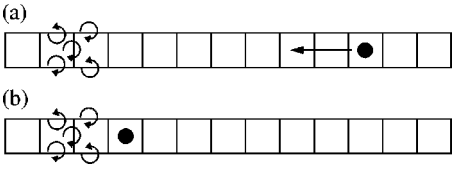

FIG. 4. (a) Ladder array with a breather and an approaching vortex. (b) At a later time, the vortex is pinned by the breather.

III. VORTEX-BREATHER COLLISIONS

To study the interaction between a single vortex and the DB we have used a ladder array with 60 cells. We have done numerical simulations of Eqs. (2) using a fourth-order Runge-Kutta algorithm in the absence of noise and a third-order one for integrating the stochastic problem.[22] In this section we will present simulations in the deterministic limit (zero temperature).

We have found four main scenarios when increasing the external bias current. (i) At the lowest current, the vortex collides with the breather and gets pinned to it. In this case the breather is acting as a pinning center for the single vortex (Figs. 4 and 5). (ii) As the current increases, the vortex causes some of the vertical junctions to switch and it thereby excites multisite breathers in its wake. The vortex eventually collides with the breather and in the resulting interaction the vortex escapes the ladder (Fig. 6). (iii) At still larger current, the vortex causes all of the vertical junctions in its wake to rotate. The resultant state is a whirling mode front which collides with the breeather, and due to this interaction the front ceases to propagate (Fig. 7). (iv) At higher values of the bias, the vortex, accompanied by the excited whirling front, collides with the breather and annihilates it (Fig. 8).

In our simulations, a breather is initially placed in vertical junction 11 and a single vortex is placed at junction 47, so both are far enough from the edges of the array. $T=0$ and we start with an applied current $i_{\rm ext}=0.45$. In this situation the vortex moves toward the breather.

We can look at the phases to get information on the dynamics of the array. Figure 4(a) sketches the situation when the vortex is approaching the breather. The solid circle shows the vortex location and the arrows the rotating junctions associated with the breather. At this moment, the vortex is eight cells from the breather. At a later time, the vortex collides with the breather and it gets pinned. If the breather is centered in vertical junction 11, the vortex gets pinned between vertical junction 12 and 13 as shown in Fig. 4(b). (Also, although is not showed in the figure, two moving vortices can be used to describe the DB dynamics.[13])

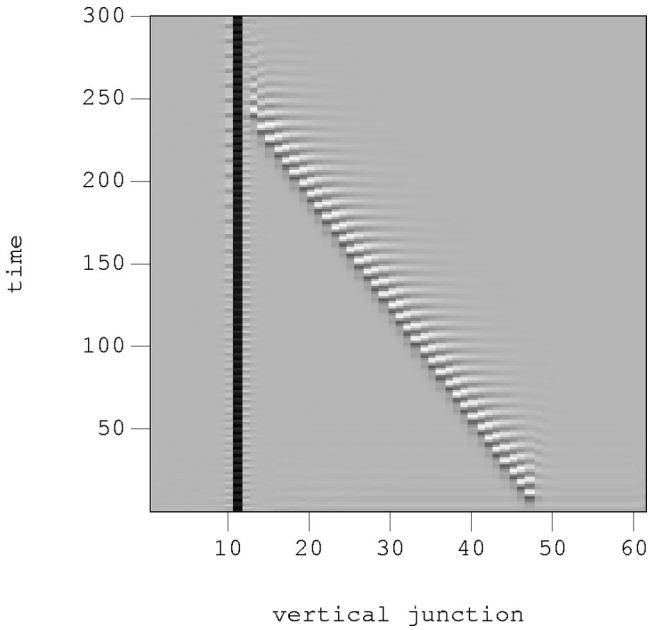

FIG. 5. Vertical junction instantaneous voltage plot of a single vortex colliding with a breather ($i_{ext}=0.45$). The final state is shown in Fig. 4(b)

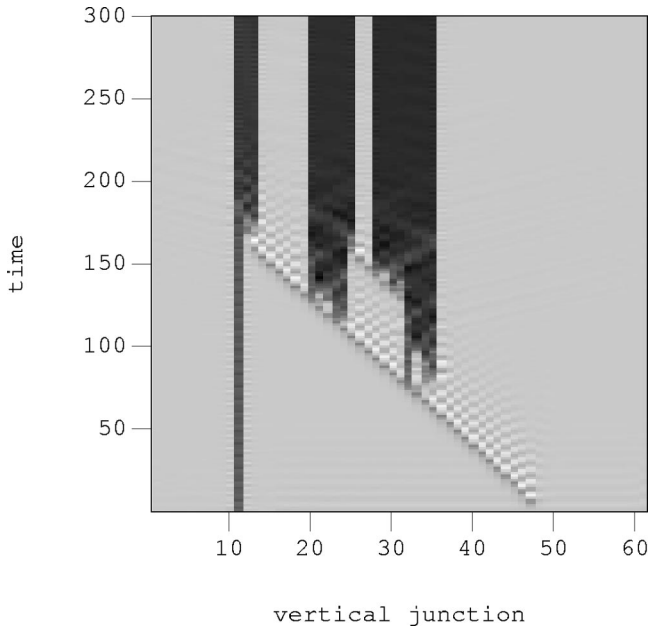

FIG. 6. Vertical junction instantaneous voltage plot of a single vortex colliding with a breather ($i_{ext}=0.5$). The moving vortex switches some of the vertical junctions to rotate. The final state shows three multisite DB's with three, six and eight vertical rotating junctions, respectively.

Another way of extracting information from the simulations is to look at the velocities of the phases—instantaneous voltages—of the vertical junctions. Figure 5 plots these voltages as a function of time; the darker regions represent higher voltages. Far from the vortex all the junctions librate around zero except the vertical junction 11 sustaining the breather which oscillates around a nonzero dc value. As the vortex moves from right to left, it creates a voltage spike every time it crosses a junction because a junction phase slip of 2π occurs. The plot shows these voltage spikes. The plot, however, does not show that the traveling vortex actually gets pinned when it collides with the breather as shown in Fig. 4(b).

If we increase the current drive above $i_{ext}\sim 0.5$, then single moving vortices are not stable in the array because they resonate with the L_JC resonance. Instead, some or all of the vertical junctions in the vortex wake are switched to the whirling mode.

Figure 6 shows one of these situations when $i_{ext}=0.5$. The moving vortex causes some, but not all, of the vertical junctions to switch to the rotating mode. These jumps in fact corresponds to the excitation of multisite DB's in the ladder. At time $\simeq$170 the vortex collides with the breather. After this collision, the vortex escapes the ladder, but the result of the interaction is now a three-site breather state located in junctions 11–13. We can see that now the steady state of the ladder corresponds from right to left in the figure to a eight-site DB with junctions 28–35 rotating, a six-site DB located in junctions 20–25, and a three-site DB located in junctions 11–13. This scenario is dependent on the initial conditions and other simulation parameters, but it is still interesting to note that at the transition between a stable moving vortex and a propagating whirling mode, a moving vortex can excite breathers in the ladder.

At higher values of the external current the moving vortex excites to the rotating state all the vertical junction in its wake. Now, instead of multisite breathers, the result is a whirling mode front which advances excited by and associ-

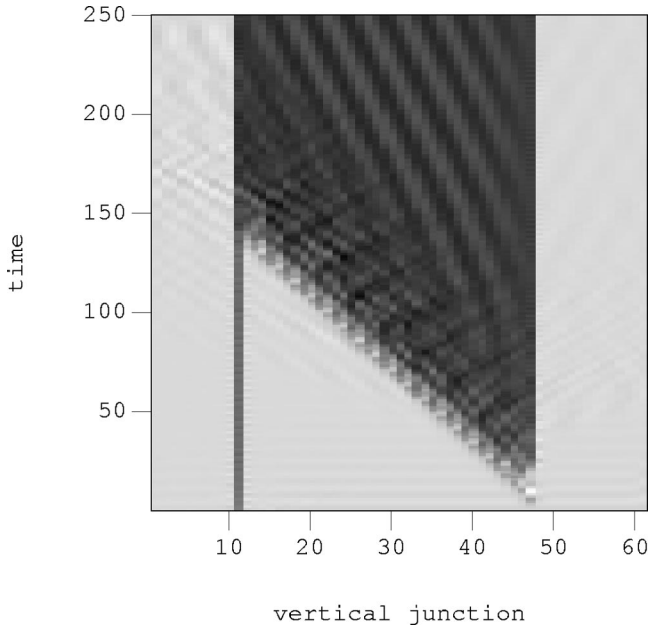

FIG. 7. Vertical junction instantaneous voltage plot of a single vortex colliding with a breather ($i_{ext}=0.55$). The moving vortex switches all of the vertical junctions to rotate. In the final state all the vertical junctions between the initial position of the vortex and the breather are in the whirling state, while the others are in the superconducting state.

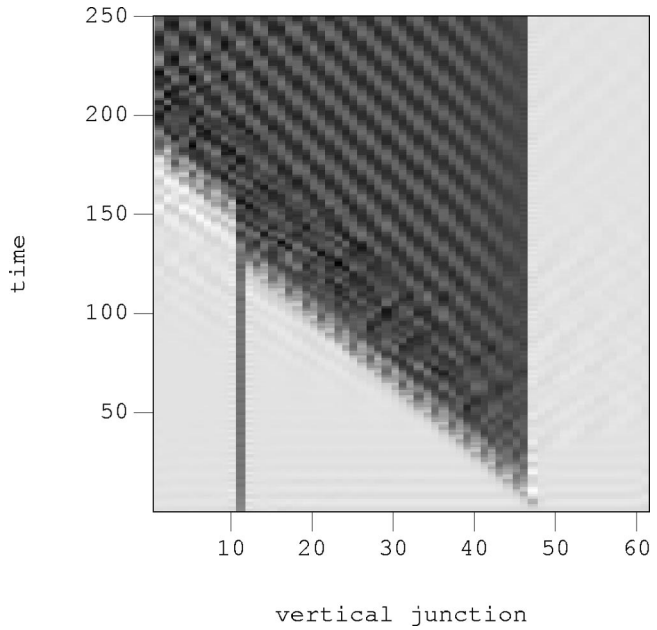

FIG. 8. Vertical junction instantaneous voltage plot of a single vortex colliding with a breather ($i_{\text{ext}}=0.59$). The vortex switches all of the vertical junctions in its wake and annihilates the breather.

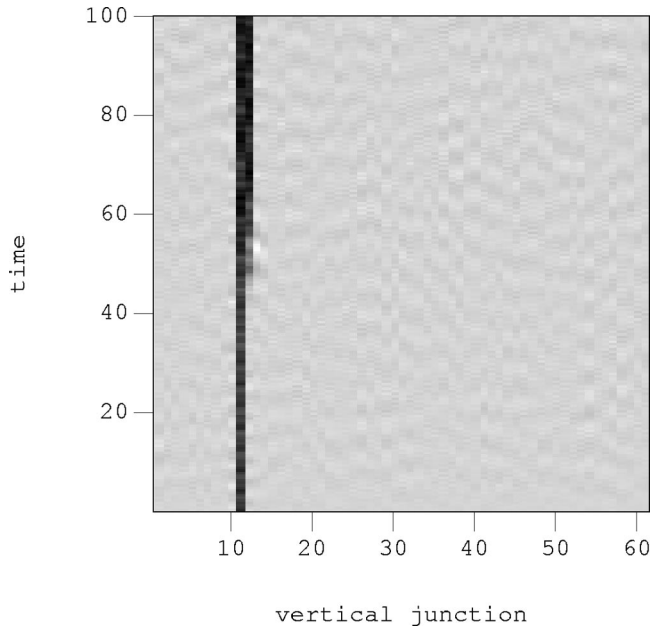

FIG. 9. Simulation with temperature of a breather in junction 11 and a pinned vortex next to it [Fig. 4(b)]. At time ~50, the vortex depins and interacts with the single-site breather to form a two-site breather.

ated with the vortex. Figure 7 shows the result of a simulation with $i_{\text{ext}}=0.55$. At this applied current, the whirling mode front collides with the breather and the resulting interaction destroys the single site breather at junction 11 and it causes the front propagation to stop. The resulting final state is that all the junctions between the initial position of the breather, junction 11, and the initial position of the vortex, junction 47, are in the resistive state meanwhile the other junctions are in the superconducting state. In fact, such a state corresponds to a large multisite DB which extends from junction 11 to junction 47.

Figure 8 shows the result of a simulation if we increase the current drive further. At $i_{\text{ext}}=0.59$ the vortex and excited front collide with the breather and destroy the breather. The vortex and whirling mode front continue to travel through the array until all the array to the left of the initial position of the vortex is in the whirling state with all these vertical junctions rotating.

IV. ENERGY BARRIER ASSOCIATED WITH THE VORTEX-BREATHER PAIR

We have seen (Figs. 4 and 5) that if the current drive is small enough, the DB appears to act as a pinning center. If we consider the effects of additive noise, then a fluctuation may cause the vortex to overcome the breather energy barrier and so the breather and vortex can combine in some fashion. Equivalently, in general, a trajectory in phase space may move from one basin of attraction to another under the presence of noise. We are both interested in the mean escape time from the basin of attraction that corresponds to Fig. 4(b), which is a vortex pinned by a breather and the final state after the vortex interacts with the breather.

In systems under equilibrium, the rate of escape from a potential well is given by an Arrhenius formula

$$\tau(T)=\tau_a e^{E_a/k_b T}, \tag{3}$$

where E_a is the height of the potential barrier and is generally referred to as an activation energy. The time $\tau(T)$ is called the lifetime at a given T, and τ_a^{-1} is the attempt frequency. Equation (3) is usually derived from a low-temperature limit, so it is accurate at small temperatures.

In dynamical systems that are not in equilibrium, the problem can be generalized to thermal escape from an attractor that may not necessarily be a fixed point. For instance, our DB is not a fixed point, but rather a limit cycle with some periodicity. In this case, thermally induced escape can also be modeled by Eq. (3). The notion of an activation energy can be interpreted as the minimum energy required to move a noise-free trajectory to the boundary of its attractor.

In the following, we will numerically calculate the activation energy by performing stochastic simulations and develop a simple model that gives an order-of-magnitude estimate for the activation energy.

In order to take into account thermal effects in the system we included in our model for the dynamics a Johnson noise current source $I_j^N(t)$ with $\langle I_j^N(t)I_j^N(t')\rangle=2kT/R_j\delta(t-t')$. After normalizations, the value for the dimensionless temperature (see Sec. II) is $\tilde{T}=kT/E_J$. For typical junctions, $I_{cv}=96\,\mu$A/h where $h=0.5$. Then $E_J=4.5\times10^3$ K and with this normalization 4.2 K equals $\tilde{T}\approx9.3\times10^{-4}$.

We have done simulations of the ladder with an added Johnson noise. We start our simulation with the initial condition shown in Fig. 4(b). This is a steady-state solution where the vortex is pinned next to the breather. We then integrate our ladder equation with the added noise sources

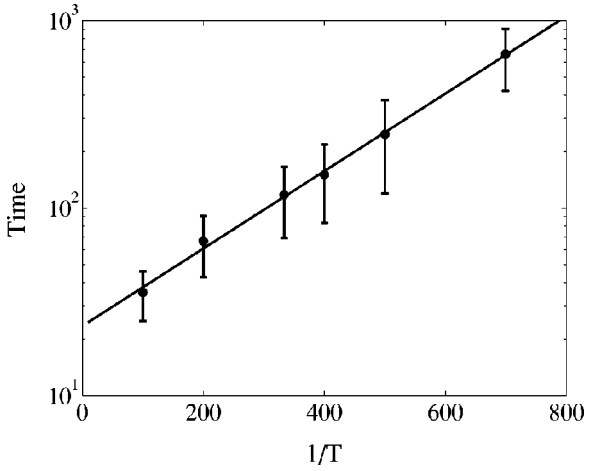

FIG. 10. Escape time for the vortex as a function of $1/T$. The slope of $E_a=0.0048$ is the activation energy. Error bars represent distribution of times within one standard deviation of the mean value.

until the vortex overcomes the barrier and combines with the breather. Figure 9 shows the plot of a simulation with noise of a breather in junction 11 and a pinned vortex. We have set our normalized temperature to 5×10^{-3}. We see that in this particular simulation at time equal to 50 the vortex overcomes the barrier and the single-site breather becomes a two-site breather. The final state depends on the temperature. Sometimes the single breather turns into an m-site breather with $m>2$. If the temperature is large, then the vortex can escape through the top horizontal junction and thereby not interact with the breather. At the low normalized temperature of $<5\times10^{-3}$ the breather and vortex almost always form a two-site breather after a finite amount of time.

At any given temperature, there will be a distribution of times for the vortex to depin. Numerically, we can define this depinning event when the junction separating the vortex and the breather slips over π. In this way we are able to calculate a series of histograms for a given temperature.

Figure 10 plots the average escape time for the vortex as a function $1/T$. Each temperature is the average of hundreds of events. The slope of this line is the activation energy and is equal to $E_a=0.0048$. Also, $\tau_a=23.5$. We can now calculate the lifetime of the pinned vortex. For example, the lifetime of the vortex at 4.2 K is $\tau=23.5e^{0.0048/0.00046}\approx4\times10^3$ in normalized units.

To find the unnormalized values, we use typical experimental parameters. The maximum critical current is $I_c=(96\,\mu\mathrm{A})/h$, and the capacitance is $C=360\,\mathrm{fF}/h$. Also, for these simulations $h=0.5$. Our equations have time normalized by $1/\sqrt{L_JC}\approx0.9\times10^{12}$. Therefore the lifetime at 4.2 K is 4.4×10^{-9} seconds or $\sim$225 MHz. This lifetime will be smaller (and the corresponding frequency larger) as the temperature is increased. Conversely, at $T=300\,\mathrm{mK}$ the lifetime is longer than the age of the universe. Also, the unnormalized activation energy is $E_a=22\,\mathrm{K}$.

To develop a simple model it is instructive to plot the phase of vertical junction 12: that is, the junction that separates the vortex from the breather when the vortex is pinned by the breather [Fig. 4(b)]. Figure 11 shows the phase as a function of time. When the breather is essentially isolated, this phase oscillates at a mean value of 0.058π. When the vortex becomes pinned by the breather at about $t\sim120$, the mean phase increases by 0.41π to 0.467π.

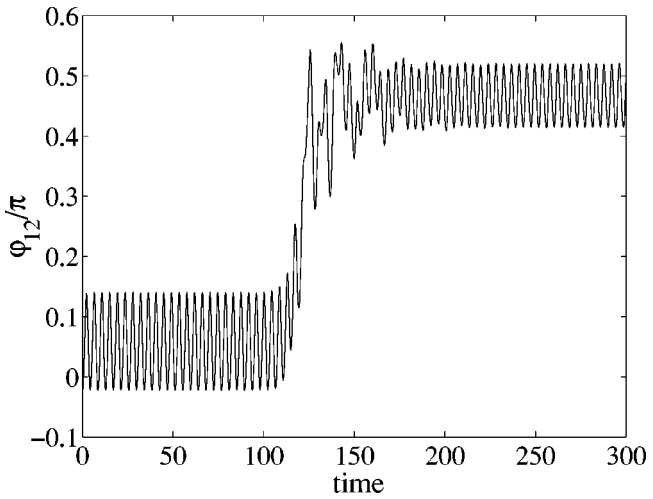

FIG. 11. Time evolution of the phase of vertical junction 12 between the pinned vortex and the breather.

Figure 12 shows the circuit diagram of the breather. We will estimate the mean phase $\langle\varphi_{12}^v\rangle=\varphi^r$ by using a dc circuit approximation. Then $v^t=v^l/2$ implies $i^t=hi^l/2$. Using current conservation in node a, $i_{\mathrm{ext}}=2i^t+i^l$, we get

$$i^t=\frac{h}{2h+2}\,i_{\mathrm{ext}}. \tag{4}$$

We can also assume that far from the breather, the current of the vertical junctions is uniform and equal to i_{ext}.

We let the current of the first quiet vertical junction to the right of the breather be $\sin\varphi^r$, $i^h=h\sin\varphi^h$ is the current of the horizontal junction, and, as an approximation, the next quiet vertical junction current is i_{ext}. We apply current conservation at node b,

$$\sin\varphi^r=i^t-i^h+i_{\mathrm{ext}} \tag{5}$$

and, using Eq. (4),

$$\varphi^r=\sin^{-1}\left(\frac{3h+2}{2h+2}\,i_{\mathrm{ext}}-h\sin\varphi^h\right). \tag{6}$$

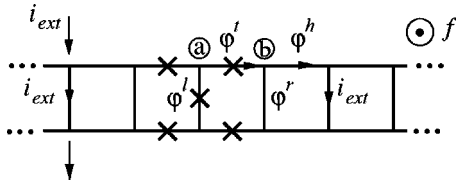

FIG. 12. Breather circuit diagram. The rotating junctions are marked by an "×": other quiet junctions are marked by shorts. All of the vertical junctions in the array are biased by the external current.

To satisfy fluxoid quantization far from the breather where the currents are uniform, φ^h must be πf. We take $\varphi^h = \pi f$ as a first approximation, and substituting the parameters of the simulations into Eq. (6), $\varphi^r = 0.038\pi$.

A better approximation can be made by taking flux quantization of the cell into account,

$$\varphi^r - \sin^{-1} i_{\rm ext} - 2\varphi^h = -2\pi f, \tag{7}$$

where we have neglected the induced flux in this cell (this flux is exactly zero in the $\lambda = \infty$ limit.) Then $\sin(\sin^{-1} i_{\rm ext} + 2\varphi^h - 2\pi f) = \sin\varphi^r$, but $2\varphi^h - 2\pi f$ is small, so we linearize the sine term of the left-hand side. We also substitute for the current $\sin\varphi^r$ and find

$$\sqrt{1-i_{\rm ext}^2}(2\varphi^h - 2\pi f) = \frac{h}{2h+2} i_{\rm ext} - h\sin\varphi^h. \tag{8}$$

We can solve for φ^h by linearizing the sine, and this results in

$$\varphi^h = \frac{h i_{\rm ext}/(2h+2) + 2\pi f\sqrt{1-i_{\rm ext}^2}}{h + 2\sqrt{1-i_{\rm ext}^2}}. \tag{9}$$

Substituting the parameters of the simulations, $\varphi^h = 0.82\pi f$, and from Eq. (6), $\varphi^r = 0.057\pi$, which is essentially the simulated value.

To estimate the phase increase when a vortex collides with the breather, we calculate the leading phase of the static vortex from Eq. (A2). We can solve for φ^t by first letting $\varphi^t = -\pi/2 + \delta$ and linearizing $\sin\delta$. The result is

$$\varphi^t = -\frac{\pi}{2} + \frac{i^h + h - \cos\pi f}{\sin\pi f}. \tag{10}$$

The leading phase of the vortex is just $\varphi^l = \varphi^t - \pi f - \pi$. If we let $i^h = h\sin\pi f$, then we find that $\varphi^t = -0.38\pi$ and $\varphi^l = 0.32\pi$. This is a good estimate for the static vortex. In our case the vortex is pinned against the breather, so i^h should include a current term due to the breather. We let $i^h = h\sin\pi f + \sin\varphi^t$. Then $\varphi^t = -0.35\pi$ and $\varphi^l = 0.35\pi$. There is still a problem in that in this situation we have broken the left-right symmetry so that $\varphi^l + \varphi^r \neq -2\pi$, though numerically we find that it is approximately true.

As a rough estimate, $\varphi^l = 0.35\pi$ is how much the phase of the vertical junction 12 increases when the vortex collides with the breather. Our rough estimate for the final phase value is $(0.057 + 0.35)\pi \approx 0.41\pi$, which is 90% of the simulated value.

To estimate the activation energy, we calculate how much energy is needed to make the junction reach its critical current. This will be of the order of $E = L_J I^2/2$. To reach the critical current the phase must equal $\pi/2$. Let $\Delta\varphi = \pi/2 - \langle\varphi_{12}\rangle$, which will in general be small. In terms of the current it is $\sin\Delta\varphi \approx \Delta\varphi$ and the energy is simply the linearized Josephson energy $E_a = L_J(\Delta\varphi)^2/2$. Using the simulated values $\Delta\varphi = 0.0033\pi$, we find that $E_a \approx 0.005$, which is what was calculated in Fig. 10.

With this phenomenological model, it should be possible to find the activation energies for other parameters and other vortex-breather states without the need to do time-consuming stochastic simulations.

V. CONCLUSION

We have studied, by means of numerical simulations, different scenarios of the collision between a moving vortex and discrete breather in a Josephson-junction ladder array. We found that it is possible for them to coexist and constructed phenomenological models so as to derive expressions for the bounds of the coexistence region. Single vortices have a maximum velocity associated with the $L_J C$ resonance of the ladder and breathers have a minimum damping and current. By a careful choice of the parameters we have managed to numerically collide traveling vortices with breathers.

We find that at some values of the parameters the discrete breathers act as pinning centers for moving vortices. After vortices get pinned by the breather, they interact with the breather when thermally activated. We have calculated this activation energy for a set of array parameters. For typical experimental values, we find that the activation energy is $E_a = 22$ K.

One possible future experiment would be to use a scanning superconducting quantum interference device (SQUID) microscope to image this interaction. The array would be imaged first when only the breather is excited and then after a vortex has been injected in the ladder. Depending on the parameters and temperature, a vortex would either become pinned or would collide and interact with the breather.

Also, other states could be excited to test the scenarios shown in the previous sections. Briefly, these scenarios correspond to the excitation by the vortex of multisite breathers in its wake and the excitation by the vortex of a whirling mode front. In the latter case, depending on the intensity of the external current, the breather either impedes the propagation of the front or is destroyed as the front propagates.

ACKNOWLEDGMENTS

This work was supported by the NSF (DMR-9988832), DGES (PB98-1592), EU (HPRN-CT-1999-00163, LOCNET), and the Commission for Cultural, Educational and Scientific Exchange between the United States of America and Spain.

APPENDIX A: SINGLE VORTEX IN A LADDER

In this appendix we review some of the properties of a single vortex in a Josephson ladder. The ground-state problem and the static properties of a JJ ladder[16–18] are similar to those of the Frenkel-Kontorova or discrete sine-Gordon (DSG) model. There exists, however, some important differences. For instance, depending on the value of λ, there exists a critical field f_c for which, if $f < f_c$, a single vortex is not stable in the ladder. At large values of λ, if the field is smaller than the critical value, the vortex is expelled from the ladder through the horizontal junctions. At smaller values of

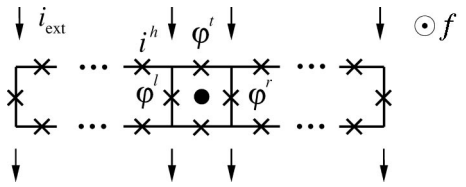

FIG. 13. A vortex in an anisotropic ladder. The large solid circle represents a vortex.

λ, self-field effects are more important in the ladder and vortices are stable at any value of the field. The critical value of λ for which this stability transition occurs is $\lambda \simeq 1$ in an array with $h=1$.[17]

Sometimes it is physically acceptable to reduce the equations of the ladder [Eqs. (2)] to a simpler expression. For instance, when studying static solutions, if we use current conservation and linearize the phases of the horizontal junctions around the solution, expressions for the $\varphi_j^{t(b)} - \varphi_{j-1}^{t(b)}$ terms are obtained. Linearizing around $\varphi_j^h = 0$, we get

$$\mathcal{N}(\varphi_j^v) = \frac{h\lambda}{h+2\lambda}(\varphi_{j+1}^v - 2\varphi_j^v + \varphi_{j-1}^v) + i_{\rm ext}. \qquad \text{(A1)}$$

This is the DSG equation with a renormalized discreteness parameter of $\lambda_{\rm eff} = h\lambda/(h+2\lambda)$ and is equivalent to the governing equations of a Josephson-junction parallel array. In the presence of an external field we can linearize around $\varphi_j^t = -\varphi_j^b = \pi f$ and we get a similar expression where now $\lambda_{\rm eff} = h\cos(\pi f)\lambda/[h\cos(\pi f)+2\lambda]$.

Figure 13 shows a schematic of the ladder. If we place a static vortex in a ladder that can be approximated by Eq. (A1), its core will be in one cell, but the vortex will extend over a length roughly determined by $\lambda_{\rm eff}$. If $\lambda_{\rm eff}$ is small, then most of the vortex properties will be determined from this core cell. The interesting thing about the ladder and these square geometries in general is that $\lambda_{\rm eff}$ is bounded by $h/2$ in the $\lambda = \infty$ limit. So in some sense the vortex is always localized. This is in contrast to the parallel array where the vortex size is unbounded. It is worth reiterating that in square geometries where every branch has a Josephson junction λ is *not* the size of the vortex (unless λ is small and $h=1$).

Suppose we place a vortex in the middle of the ladder as depicted in Fig. 13. We first want to know if the vortex will be stable. The criterion for stability is that the applied field must be greater than some critical field f_c; otherwise, the vortex will escape through the horizontal junction. We can do a rough estimation for this field working in the large-λ limit. We will see that this calculus is valid at small values of h.

Current conservation at the top left node of the core cell of the vortex in Fig. 13 yields $i^h = \sin\varphi^l + h\sin\varphi^t$, when the bias currents are zero. We will assume up-down symmetry, so $\varphi^t = -\varphi^b$, and also a left-right symmetry $\varphi^l = -\varphi^r \bmod(2\pi)$. Or $\varphi^l + \varphi^r = -2\pi$ for a positive vortex. From fluxoid quantization of the cell with the vortex, we then find that $\varphi^l = \varphi^t - \pi f - \pi$ in the $\lambda \to \infty$ limit. Current conservation on the top node can now be written as

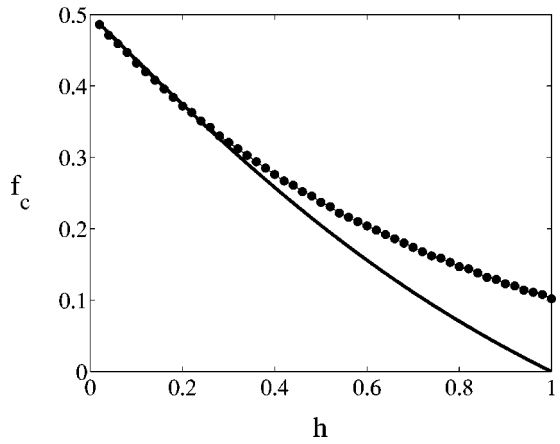

FIG. 14. Critical field needed to allow a single vortex to exist in a ladder. Solid circles are numerically calculated from full ladder dynamics with $\lambda = 5$. Solid line is the theoretical result from Eq. (A3).

$$i^h = h\sin\varphi^t - \sin\varphi^t\cos\pi f + \cos\varphi^t\sin\pi f. \qquad \text{(A2)}$$

To solve for f_c we need to know i^h. Far from the vortex core, the vertical junctions are zero and fluxoid quantization is satisfied when $\varphi^h = \pi f$. This results in a circulating current of $h\sin\pi f$. As an approximation we let $i^h = h\sin\pi f$.

If the vortex is to escape the array through the top junction, then φ^t must be $-\pi/2$. We can then solve for the critical f in Eq. (A2),

$$f_c = \frac{1}{\pi}\sin^{-1}\left(\frac{1-h^2}{1+h^2}\right). \qquad \text{(A3)}$$

In reality, i^h is not exactly $h\sin\pi f$, but as long as h is small so that $\lambda_{\rm eff}$ is small and the vortex is localized, then the effect of i^h will also be small.

Figure 14 shows a comparison of Eq. (A3) and the numerically calculated f_c for a ladder when $\lambda = 5$. The numerical calculations where performed by placing a vortex in the static equations when $f = 0.5$. Then we reduce f while tracking the eigenvalues of the Jacobian. Whenever an eigenvalue becomes greater than one then the underlying fixed point becomes unstable. The value of f where single vortex loses stability is f_c. Figure 14 shows that the approximate calculated f_c is fairly accurate only when $h < 0.5$.

Many of the properties of a vortex in the ladder are related to the existence of a pinning barrier. All Josephson arrays present a pinning barrier to the single-vortex motion.[23] The depinning current sets a lower limit on the applied current needed to move a vortex.

This depinning current can be estimated from our single-cell analysis when the vortex is highly localized. Now the analysis becomes more difficult because, by applying a current and a field, we lose the left-right mirror symmetry of the solutions. However, we will still explore the similarities between the ladder and the DSG system to study the vortex depinning current. Figure 15 shows the depinning current for the DSG equation as a function of $\lambda_{\rm eff}$. We see that when $\lambda_{\rm eff}$

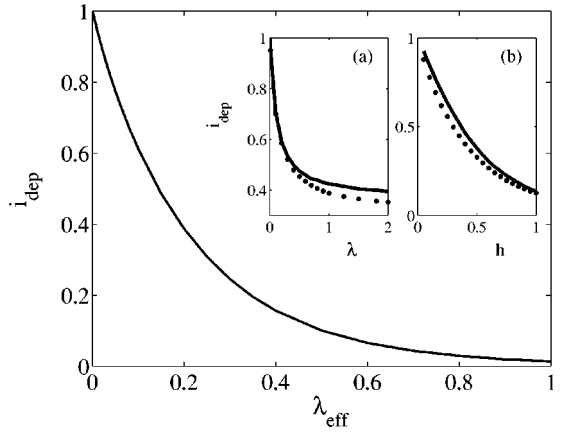

FIG. 15. Depinning current for a sine-Gordon equation as a function of the square of the penetration depth ($\lambda_{\rm eff}$). Solid circles in insets (a) and (b) are numerically calculated depinning currents of ladder when (a) $h=0.5$ and (b) $\lambda=5$. Solid lines are from the sine-Gordon equation using the $\lambda_{\rm eff}$ value.

is zero, the depinning current is 1 and in the large $\lambda_{\rm eff}$ limit the depinning current goes to zero.

We will now compare this vortex depinning current to the depinning current of a vortex in the ladder. Solid circles in Fig. 15(a) show $i_{\rm dep}$ as a function of λ when $h=0.5$ for the ladder. We have placed a vortex in the middle of the array and found the current where the pinned state loses stability. To compare this numerical result to the DSG, first we calculate a $\lambda_{\rm eff}$ for each point and then the corresponding $i_{\rm dep}$ for the DSG. The solid line is $i_{\rm dep}$ calculated from the equivalent $\lambda_{\rm eff}$ of the DSG. We see that the $\lambda_{\rm eff}$ estimation gives a very good approximation at this value of h.

Figure 15(b) shows the numerically calculated $i_{\rm dep}$ for a vortex in the ladder as a function of h when $\lambda=5$. Again, for every point we can calculate a $\lambda_{\rm eff}$ and the corresponding depinning current from the DSG equation. This is plotted as the solid line. We see that the $\lambda_{\rm eff}$ results in good approximation.

Figure 15 shows that we can estimate the depinning current of a ladder by using a single parameter $\lambda_{\rm eff}$.

Once the vortex depins, it can move through the ladder. The vortex dynamics in this regime is analogous to that of a massive particle traveling through a viscous medium.[24] The current serves as the force, the capacitance energy is analogous to the mass of the vortex, and the viscosity represents the energy loss of the vortex to the array. There are two parallel channels that lead to a viscous drag. One is the energy dissipated by the resistors as the voltage profile of the vortex passes through the junctions. The other is the energy lost through the ripples in the vortex wake that are sometimes referred to as spin waves.

In an infinite array, as the current increases the velocity of the vortex increases until the vortex becomes unstable. In general, the vortex becomes unstable when it excites a resonance in the array. For instance, in a parallel array, the vortex excites the L_sC resonance. However, in square arrays like our ladder, there are two resonances L_sC and L_JC:[13]

$$\omega^2_{L_sC}=F+\sqrt{F^2-G}, \tag{A4}$$

$$\omega^2_{L_JC}=F-\sqrt{F^2-G}, \tag{A5}$$

where $F=[1+2\lambda/h+4\lambda\sin(z/2)^2]/2$ and $G=4\lambda\sin(z/2)^2$ and from physical grounds we expect the wavelength to be well approximated by $z=2\pi f$, i.e., the average distribution of vortices in the array.

The L_JC resonance occurs at smaller frequencies. Thereby, it gets excited first in the square array.[25] Therefore, a vortex becomes unstable when the ripples in the wake excite the L_JC resonances of the junctions. Depending on Γ and h, this sets an upper limit of the applied current where a localized vortex can dynamically exist.

APPENDIX B: VORTEX AND BREATHER EXISTENCE REGION

We now have a way of calculating the parameter regime where a vortex is stable and what its maximum traveling velocity is. We will do a similar analysis for the discrete breather.

For the breather to exist in the array, the junctions must be underdamped. This sets a limit on Γ. The minimum current and maximum current for the the breather have been calculated.[13] The maximum current is

$$i_+=\frac{h+1}{2h+1}, \tag{B1}$$

while the minimum current is

$$i_-=2(h+1)\frac{4}{\pi}\Gamma. \tag{B2}$$

We will use $\Gamma=0.1$. This an an experimentally realizable value and most of the ladder arrays we have measured have approximately this damping. Also, for $f<f_c$, the single vortex is unstable in the array. Since we want to study vortex breather collisions, we choose $f=0.3$ so as to provide a large enough barrier for the vortex to remain in the ladder. This implies from Eq. (A3) that $h>0.3$. We let $h=0.5$.

There is still the choice of λ. Figure 3 shows the existence region of a breather and vortex in ladder. The solid circles in Fig. 3 show simulation results for a ladder with periodic boundary conditions with an initial condition of a single pinned vortex. As the current increases, the vortex first becomes depinned at $i_{\rm dep}$. As the current increases, it destabilizes at $i_{\rm ext}\simeq 0.5$ when the moving vortex resonates with the L_JC resonance. The solution then evolves into a whirling mode front so that above this maximum current the array does not support a single moving vortex. The hatched region in Fig. 3 shows the parameter space where a single moving vortex can exist in the array.

As λ decreases, the pinning barrier increases as expected from Fig. 15, but the maximum vortex current stays relatively unchanged. The horizontal dashed line at $i_{\rm ext}=0.52$ is calculated from assuming that the flux-flow resistance is $2f$ and the I-V is $v=(2f)(i_{\rm ext}-i_{\rm dep})$ where v is the L_JC reso-

nance and we solve for $i_{\rm ext}$. This is a rough calculation since the flux-flow resistance should increase as λ goes to zero. To approximate, we take the $\lambda \to \infty$ limit, so we use $i_{\rm dep}=0.36$ and 2 f for the flux-flow resistance. Since $i_{\rm dep}$ increases as λ goes to zero, we expect the maximum current to increase as well, but the flux-flow resistance also increases and this will tend to reduce this maximum current. Therefore, the maximum current increases at a slower rate than the depinning current. This implies that there is a critical value of λ where the array does not allow a moving vortex. The minimum λ for these parameters appears to be ~0.4 and can be estimated from the intersection of the L_JC resonance and $i_{\rm dep}$ curves.

Figure 3 also shows the existence region for the symmetric type of breathers. The bottom solid line at $i_{\rm ext}=0.38$ is the minimum current that is expected from the retrapping mechanism, Eq. (B2). The top solid line at $i_{\rm ext}=0.91$ is the maximum current current of the breather, Eq. (B1). The two curving dashed lines are the L_sC resonances. There are two branches because the horizontal junction rotates at half the voltage of the vertical junction. Thus resonances occurs when v or $v/2 \simeq \omega_{L_sC}$. To convert from the resonant voltage to current, we have used the approximate equation of the I-V.[13] In the figure we have also marked three different DB solutions:[21] B1α is the breather solution when the L_sC resonances is above the junction voltages, B1β exists when the L_sC resonance are between the voltage of the vertical and horizontal junction, and B1 is the solution when the L_sC resonance are below the array the voltages. There is also a region in Fig. 3 that allows for aperiodic breathers, but in order to simplify the graph it is not shown.

The main point of Fig. 3 is that there is a region in the parameter plane where a DB can coexist with a single vortex in a ladder. It is this overlap that allows us to study interactions between breathers and vortices. This overlap will change with the parameters. For instance, if we increase h, then the depinning current would decrease, but the retrapping current of the breather would increase so the overlap existence region would be smaller. In this paper we have presented some results of interaction between breathers and vortices and to avoid any effects of the resonances we fixed $\lambda=5$.

[1] A. Scott, *Nonlinear Science: Emergence & Dynamics of Coherent Structures* (Oxford University Press, Oxford, 1999).

[2] A. J. Sievers and J. B. Page, in *Dynamical Properties of Solids VII*, edited by G. K. Horton and A. A. Maradudin (Elsevier, Amsterdam, 1995), p. 137.

[3] S. Aubry, Physica D **103**, 201 (1997).

[4] S. Flach and C. R. Willis, Phys. Rep. **295**, 182 (1998).

[5] A. Barone and G. Paterno, *Physics and Applications of the Josephson Effect* (Wiley, New York, 1982).

[6] K. K. Likharev, *Dynamics of Josephson Junctions and Circuits* (Gordon and Breach, Amsterdam, 1986).

[7] A. V. Ustinov, Physica D **123**, 315 (1998).

[8] S. Watanabe, H. S. J. van der Zant, S. H. Strogatz, and T. P. Orlando, Physica D **97**, 429 (1996).

[9] A. van Oudenaarden and J. E. Mooij, Phys. Rev. Lett. **76**, 4947 (1996).

[10] E. Trías, J. J. Mazo, and T. P. Orlando, Phys. Rev. Lett. **84**, 741 (2000).

[11] P. Binder, D. Abraimov, A. V. Ustinov, S. Flach, and Y. Zolotaryuk, Phys. Rev. Lett. **84**, 745 (2000).

[12] P. Binder, D. Abraimov, and A. V. Ustinov, Phys. Rev. E **62**, 2858 (2000).

[13] E. Trías, J. J. Mazo, A. Brinkman, and T. P. Orlando, Physica D **156**, 98 (2001).

[14] J. J. Mazo, E. Trías, and T. P. Orlando, Phys. Rev. B **59**, 13604 (1999).

[15] L. M. Floría and J. J. Mazo, Adv. Phys. **45**, 505 (1996).

[16] J. J. Mazo, F. Falo, and Luis M. Floría, Phys. Rev. B **52**, 10 433 (1995).

[17] J. J. Mazo and J. C. Ciria, Phys. Rev. B **54**, 16 068 (1996).

[18] M. Barahona, S. H. Strogatz, and T. P. Orlando, Phys. Rev. B **57**, 1181 (1998).

[19] This is true when neglecting induced fields in the ladder ($\lambda \to \infty$). At finite λ there exists also a critical value of this parameter for which, if $\lambda < \lambda_c$, single vortices are stable in the ladder at zero external field. This $\lambda_c \sim 1$ when $h=1$ (Ref. 17).

[20] This estimation neglects the effect of λ in the dynamics. More complete analysis can be found in Ref. 13 and A. E. Miroshnichenko *et al.*, Phys. Rev. E **64**, 066601 (2001).

[21] In all cases they are single-site DB's with four horizontal junctions rotating. We have followed the notation introduced in Ref. 13.

[22] H. S. Greenside and E. Helfand, Bell Syst. Tech. J. **60**, 1927 (1981).

[23] Strictly speaking, a discrete sine-Gordon system will have a zero pinning at $\lambda=\infty$. For any finite λ there will be some pinning barrier, though vanishingly small, as λ becomes large.

[24] J. C. Ciria and C. Giovannella, J. Phys.: Condens. Matter **10**, 1453 (1998).

[25] In the limit where h is large the ladder behaves like a parallel array and both resonances occur at the same frequency.